Alkaline-Earth Rhodium Hydroxides: Synthesis, Structures and Thermal Decomposition to Complex Oxides

Daniel S. Cook,[1] Guy J. Clarkson,[1] Daniel M. Dawson,[2] Sharon E. Ashbrook,[2] Janet M. Fisher,[3] David Thompsett,[3] David M. Pickup,[4] Alan V. Chadwick[4] and Richard I. Walton[1]*

1. Department of Chemistry, University of Warwick, Coventry, CV4 7AL, UK

*Author for correspondence, email: r.i.walton@warwick.ac.uk

2. School of Chemistry, EaStCHEM and Centre of Magnetic Resonance, University of St Andrews, North Haugh, St Andrews, KY16 9ST, UK

3. Johnson Matthey Technology Centre, Sonning Common, Reading, RG4 9NH, UK

4. School of Physical Sciences, University of Kent, Canterbury, Kent, CT2 7NH, UK

Abstract

The rhodium (III) hydrogarnets $Ca_3Rh_2(OH)_{12}$ and $Sr_3Rh_2(OH)_{12}$ crystallise as polycrystalline powders under hydrothermal conditions at 200 °C from $RhCl_3 \cdot 3H_2O$ and either $Ca(OH)_2$ or $Sr(OH)_2$ in either 12 M NaOH or KOH. Rietveld refinements against synchrotron powder X-ray diffraction (XRD) data allow the first crystal structures of the two materials to be determined. If BaO_2 is used as a reagent and the concentration of hydroxide increased to hydroflux conditions (excess NaOH) then single crystals of a new complex rhodium hydroxide, $BaNaRh(OH)_6$, are formed in a phase-pure sample, with sodium included from the flux. Structure solution from single-crystal XRD data reveals isolated octahedral Rh centres that share hydroxides with 10-coordinate Ba and two independent 8-coordinate Na sites. ^{23}Na magic-angle spinning NMR confirms the presence of the two crystallographically distinct Na sites and also verifies the diamagnetic nature of the sample, expected for Rh(III). The thermal behaviour of the hydroxides on heating in air was investigated using X-ray thermodiffractometry, showing different decomposition pathways for each material. $Ca_3Rh_2(OH)_{12}$ yields $CaRh_2O_4$ and CaO above 650 °C, from which phase-pure $CaRh_2O_4$ is isolated by washing with dilute nitric acid, a material previously only reported by high-pressure or high-temperature synthesis. $Sr_3Rh_2(OH)_{12}$ decomposes to give a less crystalline material with a powder XRD pattern that is matched to the 2H-layered hexagonal perovskite $Sr_6Rh_5O_{15}$, which contains mixed-valent $Rh^{3+/4+}$, confirmed by Rh K-edge XANES spectroscopy. On heating $BaNaRh(OH)_6$ a complex set of decomposition events takes place via transient phases.

Introduction

Oxides and hydroxides of rhodium have been rather less studied than those of other 4d and 5d metals, which may be in part due to the scarcity and expense of the metal, but also the smaller range of accessible oxidation states under moderate reaction conditions makes synthesis more challenging. Primarily trivalent, rhodium forms corundum-type Rh_2O_3, though high-temperature and high-pressure polymorphs are known.[1-3] RhO_2 can be prepared, by using high oxygen pressure,[4-5] and adopts the rutile structure, a common structure type of metal dioxides, including those of other platinum-group metals, such as RuO_2 and IrO_2. Just over ten years ago Müller-Buschbaum surveyed the various ternary and higher oxides of rhodium known at that time and this confirmed the commonplace occurence of the +3 oxidation state of rhodium, in ternary oxides such as in the double rutiles $ARhO_4$ (A = Sb, Nb, Ta) and the delafossites $BRhO_2$ (B = Na, Ag, Cu).[6] Nevertheless the +4 oxidation state can be stabilised by using the covelancy of a partner metal in a ternary oxide, such as in the hexagonal perovskite 4H-$BaRhO_3$[7] and mixed-valent $Ba_9Rh_8O_{24}$,[8] and various materials based upon the K_2NiF_4 structure, such as Sr_2RhO_4[9] and $Sr_3Rh_2O_7$,[10] although often high pressure is needed during synthesis. Exploring new synthesis conditions allows more unusual oxidation states to be accessed, for example Rh^{5+} is stablised in Sr_3MRhO_6 (M = Na, Li) by a molten alkali flux synthesis at a low temperature of 600 °C.[11] Zur Loye and co-workers have more recently prepared a number of lanthanide-platinum-group metal oxides from hydroxide fluxes, including some complex hexagonal perovskites containing rhodium.[12] In terms of properties, since Rh^{3+} is invariably octahedral and hence low-spin $4d^6$, magnetism in rhodium oxides is only found for the higher oxidation states: for example, the mixed-valent hexagonal perovskite $Sr_6Rh_5O_{15}$ ($Rh^{3+/4+}$) shows low-temperature magnetic order.[13] Some rhodates have other interesting properties arising from their electronic structure: Sr_2RhO_4 is a two-dimensional conductor,[9] while hydrated Na_xRhO_2 materials have been shown to possess favourable thermoelectric behaviour at temperatures relevant for power generation from waste heat,[14] and recently $AgRhO_2$ has been shown to be active for photoelectrochemical water splitting with visible light.[15]

We have peviously used hydrothermal chemistry to prepare a number of novel oxides of ruthenium and iridium: this makes use of very mild conditions in which metal salt precursors are heated in water at around 200 °C to crystallise polycrystalline powders of ternary oxides directly from solution.[16-18] In the case of ruthenium, a number of interesting materials were thus discovered, including the layered hexagonal honeycomb $SrRu_2O_6$, which has an abnormally high antiferromagnetic ordering temperature,[19] the oxyhydroxide $Ba_4Ru_3O_{10.2}(OH)_{1.8}$ with a novel variant of a hexagonal perovskite structure,[20] and mixed ruthenate-iridate pyrochlores that can act as electrocatalysts for oxygen evolution from water.[21] Jansen and co-workers have also used related hydrothermal conditions to prepare novel silver ruthenates.[22-23] Given the recent interest in the chemistry of platinum-group metal oxides in applications such as catalysis[24] and the wider focus on the magnetic and electronic properties of oxides of the 4d and 5d metals by the physics community,[25] we have extended our exploration of hydrothermal chemistry of such metals to rhodium. In this case, we find that hydroxides are formed, rather than oxides, but thermal decomposition of these provides a convenient route to the ternary oxide $CaRh_2O_4$, previously only prepared using extreme pressure,[26] or by heating at 1400 K in pure oxygen,[27] and a mixed oxide of Sr and Rh that contains some Rh^{4+}. To our knowledge the only report of the hydrothermal synthesis of rhodium oxides used supercritical conditions in sealed gold vessels at 600 °C and 1-2 kbar to form RhO_2 and RhOOH from Rh_2O_3 precursors.[28]

Experimental

To synthesise $Ca_3Rh_2(OH)_{12}$ 0.10 g (0.38 mmol) $RhCl_3 \cdot 3H_2O$ (Precious Metals Online, 99%) and 0.04 g (0.57 mmol) $Ca(OH)_2$ (Aldrich; 96%) were added to 10 mL 12 M KOH solution with stirring. The mixture was sealed in a 23 mL PTFE-lined steel autoclave and heated to 200 °C for 24 hours in a preheated fan oven. The autoclave was then cooled to room temperature and the resulting precipitate

was recovered by suction filtration to yield a brown powder. The material was washed with acetone and dried in air at room temperature.

$Sr_3Rh_2(OH)_{12}$ was prepared using 0.1 g (0.38 mmol) $RhCl_3 \cdot 3H_2O$ (Precious Metals Online, 99%) and 0.023 g (0.19 mmol) $Sr(OH)_2$ (Aldrich; 95%), which were added to 10 mL 12 M NaOH solution with stirring. The mixture was sealed in a 23 mL PTFE-lined steel autoclave and heated to 200 °C for 24 hours in a preheated fan oven. The autoclave was then cooled to room temperature and the resulting precipitate was recovered by suction filtration to yield a bright yellow powder. The material was washed with acetone and dried in air at room temperature.

Polycrystalline $BaNaRh(OH)_6$ was synthesised by adding 0.1 g (0.38 mmol) $RhCl_3 \cdot 3H_2O$ (Precious Metals Online, 99%) and 0.032 g (0.10 mmol) $Ba(OH)_2 \cdot 8H_2O$ (BDH; 97%) to 10 mL 12 M NaOH solution with stirring. The mixture was sealed in a 23 mL PTFE-lined steel autoclave and heated to 200 °C for 24 hours in a preheated fan oven. The autoclave was then cooled to room temperature and the resulting precipitate was recovered by suction filtration to yield a gold coloured powder. To grow single crystals of $BaNaRh(OH)_6$, 0.1 g (0.38 mmol) $RhCl_3 \cdot 3H_2O$ (Precious Metals Online, 99%), 0.032 g (0.19 mmol) BaO_2 (Aldrich; ≥95%) and 4.0 g (0.1 mol) NaOH (Fischer, ≥97%) were added to a PTFE-lined steel autoclave and 2 mL distilled water was added without stirring. The autoclave was sealed and placed in an oven set to ramp to 200 °C at 300 °C h^{-1}, held for 24 hours and then cooled to room temperature at 6 °C h^{-1}. The crystals formed were separated from the flux using hot water, aided by gentle stirring, followed by vacuum filtration with acetone used to dry the crystals.

Samples were initially screened using powder XRD measured using a Siemens D5000 diffractometer (Cu $K\alpha_{1/2}$ radiation) operating in Bragg-Brentano geometry. Non-ambient powder XRD measurements were made using a Bruker D8 Advance diffractometer equipped with Cu $K\alpha_{1/2}$ radiation and a VÅNTEC-1 high-speed detector. Powders were heated in situ using an Anton Paar XRK 900 reaction chamber controlled through a TCU 750 temperature unit. High-resolution powder XRD patterns were measured at room temperature using beamline I11 at the Diamond Light Source,

UK,[29] from samples held in thin-walled quartz capillaries with 0.82482 Å X-rays. The Multi-Analyzer Crystal (MAC) detector and the MYTHEN position-sensitive detector were used. Powder XRD patterns were analysed using the TOPAS (version 4.1) software implemented with jEdit.[30] The quality of the Rietveld fits was verified by analysing the resultant structural models using the bond-valence sum method as an independent check of the chemical plausibility of the refined crystal structures.

$BaNaRh(OH)_6$ single crystal XRD data were recorded using MoKα (λ = 0.71073 Å). A suitable crystal was selected and mounted on a glass fibre with Fromblin oil and placed on a Rigaku Oxford Diffraction SuperNova diffractometer with a duel source (Cu at zero) equipped with an AtlasS2 CCD area detector. The crystal was kept at 150(2) K during data collection. Using Olex2, the structure was solved with the ShelXT structure solution program[31] using intrinsic phasing and refined with the ShelXL refinement package[32] using least squares minimisation.

Rh K-edge X-ray absorption near edge structure (XANES) spectra were collected on Beamline B18, at Diamond Light Source, UK.[33] Samples were diluted with polyethylene powder and pressed into pellets approximately 1 mm thick to optimise absorption. Data were collected in transmission mode and spectra were normalized using the ATHENA software.[34]

Combined thermogravimetric analysis (TGA) and differential scanning calorimetry (DSC) was performed using a Mettler Toledo Systems TGA/DSC 1 instrument under a constant flow of air (50 mL min^{-1}).

Scanning electron microscopy (SEM) images were recorded using a ZEISS GEMINI. A small amount of sample was placed on to a carbon tape prior to analysis. Transmission electron microscopy (TEM) was performed using a JEOL 2000FX instrument with samples placed on holey carbon copper grids via dispersion in acetone.

The solid-state ^{23}Na NMR spectrum of $BaNaRh(OH)_6$ was recorded using a Bruker Avance III spectrometer equipped with 9.4 T wide-bore superconducting magnet. The sample was packed in a 4

mm zirconia rotor and rotated at the magic angle at a rate of 14 kHz. The magic angle spinning (MAS) spectrum was recorded with a short flip angle (~ 18°) pulse and signal averaging for 4096 transients with a recycle interval of 2 s. Spectral resolution was improved by the application of high-power continuous wave (CW) decoupling of ^{1}H during acquisition. Chemical shifts are reported in ppm relative to 0.1 M NaCl in D_2O using an external sample of solid NaCl (δ_{iso} = 7.2 ppm) as a secondary reference.

Results and Discussion

The hydrogarnets $Ca_3Rh_2(OH)_{12}$ and $Sr_3Rh_2(OH)_{12}$ have previously been reported in the literature but a full structural characterisation of each has not been undertaken. $Sr_3Rh_2(OH)_{12}$ was studied by Ivanov-Emin et al.,[35] whilst $Ca_3Rh_2(OH)_{12}$ features only in a table of silicon-free hydrogarnets published by Morán-Miguélez et al.,[36] and in each case only the cubic lattice parameter was reported. Figure 1 shows the final Rietveld fit achieved for each material and Table 1 shows the final fitted parameters. In each case, the crystal structure of $Sr_3Fe_2(OH)_{12}$[37] was used as a starting point and the variable coordinates of the oxygen positions were allow to vary along with isotropic temperature factors and the cubic lattice parameter. An impurity phase of $Ca(OH)_2$ was observed in $Ca_3Rh_2(OH)_{12}$ and this was included in the refinement as a second phase: the relative amounts of the hydrogarnet and $Ca(OH)_2$ from the Rietveld refinement were estimated as 70% and 30%, respectively, from the refined scale factors. Attempts to be prepare samples free from $Ca(OH)_2$ by using stoichiometric amounts of Ca reagent, led to Rh metal present as an impurity.

$Ca_3Rh_2(OH)_{12}$ was previously reported from a low-temperature, high-pressure hydrothermal synthesis (150 °C, 1000 bar) using rhodium oxide as the rhodium precursor.[36] Its structure, however, was not refined, with only a list of observed reflections provided. The refined lattice parameter we determine here of a = 12.76000(9) Å is similar to the value of 12.743(2) Å reported by Morán-Miguélez et al.[36] for the same composition, but smaller than that of $Sr_3Fe_2(OH)_{12}$ (a = 13.202 Å),[37] as expected for the presence of the smaller alkaline-metal cation. The refined lattice

parameter of $Sr_3Rh_2(OH)_{12}$ a = 13.18643(5) Å is only slightly smaller than that reported for $Sr_3Fe_2(OH)_{12}$ but considering that 6-coordinate high spin Fe^{3+} and 6-coordinate Rh^{3+} are similar in size (0.645 Å cf. 0.665 Å)[38] this is not unexpected; it is also very similar to the value of 13.156(2) Å reported by Morán-Miguélez et al.[36] Bond valence sums[39] confirm the presence of trivalent rhodium in the two materials, with values determined as 2.84 and 3.02 for $Ca_3Rh_2(OH)_{12}$ and $Sr_3Rh_2(OH)_{12}$, respectively.

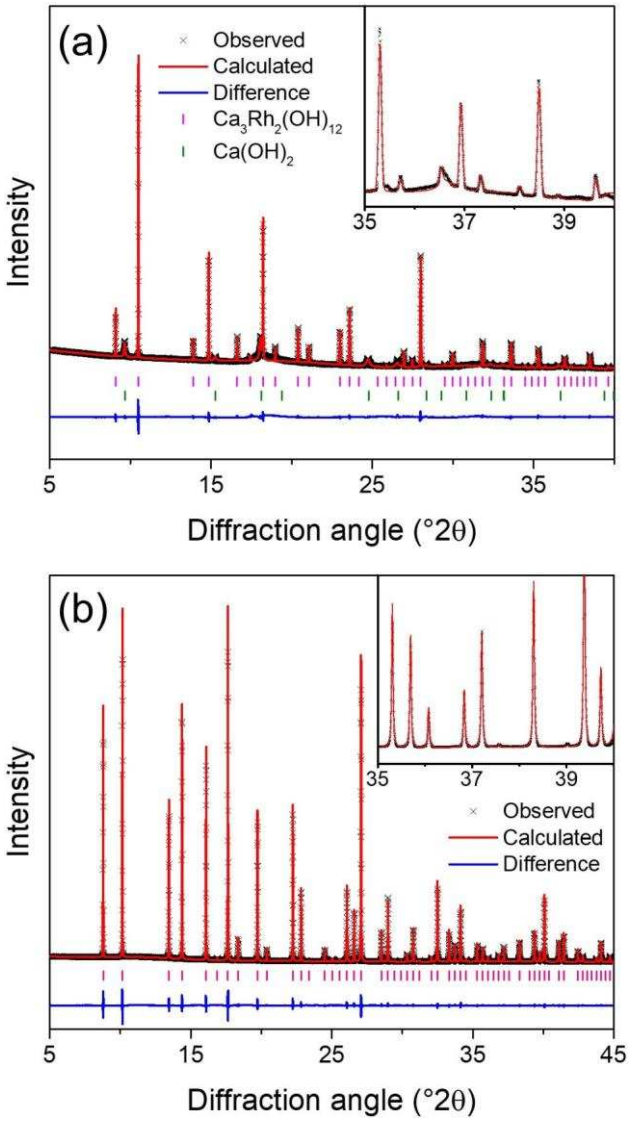

Figure 1: Final Rietveld plots (λ = 0.82482 Å) for (a) $Ca_3Rh_2(OH)_{12}$ and (b) $Sr_3Rh_2(OH)_{12}$. The insets are expanded regions of the main plots. In (a) the lower set of tick marks represent the $Ca(OH)_2$ impurity. See Table 1 for refined crystallographic parameters.

Table 1: Refined crystal data for $Ca_3Rh_2(OH)_{12}$ and $Sr_3Rh_2(OH)_{12}$ from powder XRD

$Ca_3Rh_2(OH)_{12}$. Space group $Ia\bar{3}d$, a = 12.76000(9) Å. Rp = 4.02%, wRp = 5.99%.

Wyckoff Site	Atom	x	y	z	Occupancy	B_{eq} / Å^2
16a	Rh	0	0	0	1.0	0.46(4)
24c	Ca	0.125	0	0.25	1.0	1.11(9)
96h	O	0.0319(3)	0.0598(5)	0.6472(4)	1.0	0.4
96h	H	0.180	0.081	0.789	1.0	0.4

$Sr_3Rh_2(OH)_{12}$. Space group $Ia\bar{3}d$, a = 13.18643(5) Å. Rp = 8.68%, wRp = 13.48%.

Wyckoff Site	Atom	x	y	z	Occupancy	B_{eq} / Å^2
16a	Rh	0	0	0	1.0	0.47(3)
24c	Sr	0.125	0	0.25	1.0	0.41(3)
96h	O	0.0324(2)	0.0521(3)	0.6424(2)	1.0	0.4
96h	H	0.180	0.081	0.789	1.0	0.4

*The H parameters were not refined, but set at the values for the Fe analogue.

Using CaO_2 or SrO_2 in place of the corresponding hydroxide in the hydrothermal reactions yielded the same hydrogarnets and not oxide materials, in contrast to what has been observed for other hydrothermal reactions with platinum-group metals Ru and Ir where complex oxides containing the metal in the +4 and/or +5 oxidation states are formed when peroxides are used as reagents.[18] This reflects the difficulty in oxidising Rh to the higher oxidation states. In the case of barium, a hydrogarnet was not synthesised through analogous reactions and this is likely due to the large size of the cation; indeed barium hydrogarnets have only been observed containing a larger trivalent partner metal cation, such as scandium and indium.[40] Instead, using either $Ba(OH)_2$ or BaO_2 under similar hydrothermal conditions in NaOH gave the new material $BaNaRh(OH)_6$ as a polycrystalline powder. To aid structure solution we investigated the preparation of single crystals sufficiently large

for single-crystal XRD and used conditions named ‘wet hydroflux’ by zur Loye and co-workers,[41] where a large excess of NaOH is used and a small volume of water: the excess hydroxide is readily washed away with additional water following the synthesis. Figure 2a shows an SEM micrograph of typical crystals formed by this method, while Figures 2b and 2c show views of the crystal structure.

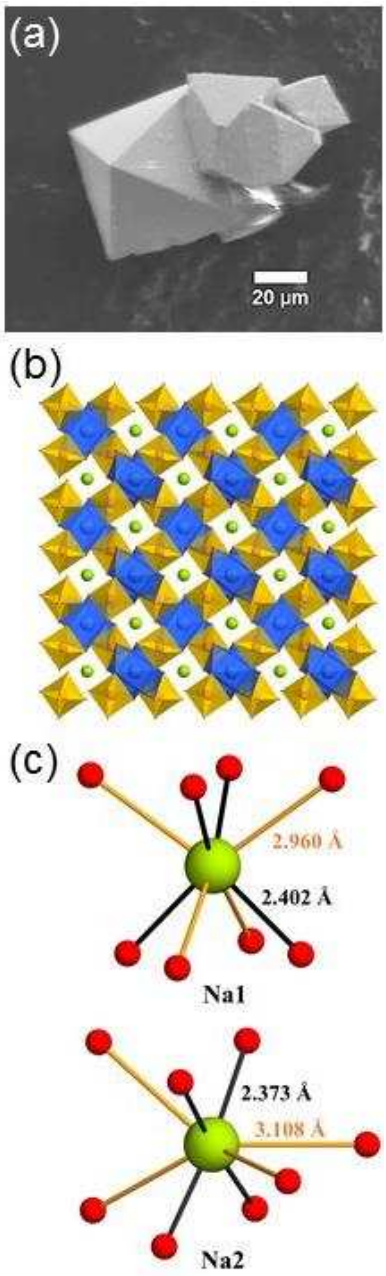

Figure 2: (a) SEM micrograph of $BaNaRh(OH)_6$, (b) view of the structure of $BaNaRh(OH)_6$ showing 6-coordinate Rh as yellow polyhedra and 10-coordinate Ba as blue polyhedra with Na as green spheres and (c) the two crystallographically distinct 8-coordinate Na sites with oxygens as red spheres and with the two pairs of bond lengths in each indicated by shading.

Table 2: Refined single crystal parameters for $BaNaRh(OH)_6$ space group $P4_2/n$, (no. 86), a = 8.28420 Å, c = 8.41980 Å.

Wyckoff site	Atom	x	y	z	Occupancy	U_{iso} / Å^2
4e	Ba	0.25	0.25	0.79014	1.0	0.009
4d	Rh	0.5	0.5	0.5	1.0	0.006
2b	Na1	0.25	0.25	0.75	1.0	0.014
2a	Na2	0.25	0.25	0.25	1.0	0.026
8g	O1	0.45356	0.26059	0.54711	1.0	0.010
8g	O2	0.44558	0.45874	0.26546	1.0	0.010
8g	O3	0.26183	0.54071	0.54598	1.0	0.011

$BaNaRh(OH)_6$ contains isolated Rh-centred octahedra that share hydroxides with 10-coordinate Ba, with Ba-O bond distances ranging from 2.69 – 3.09 Å and an average bond length of 2.86 Å, close to expected Ba-O distances in mixed-metal hydroxides.[42] Sodium occupies two different sites in the crystal structure, both with 8 coordination. The Na-O bond distances fall is two pairs: 2.402 and 2.960 Å for Na1 with an average distance of 2.681 Å, and 2.373 and 3.018 Å for Na2 with an average bond distance of 2.696 Å. Bond valence sums were used to confirm the oxidation states in $BaNaRh(OH)_6$: this gave values of 2.97, 2.08, 0.96, 1.00 for Rh, Ba, Na1 and Na2, respectively. The phase purity of the polycrystalline sample of $BaNaRh(OH)_6$ was confirmed using powder XRD (Supporting Information) while ^{23}Na solid-state NMR spectroscopy was used to verify the presence of two Na sites in the material, as shown in Figure 3. Two resonances are observed with isotropic chemical shifts (δ_{iso}) of 0.7 and –0.2 ppm, consistent with 8-coordinate Na. However, the quadrupolar coupling constants (C_Q) of the two resonances are very different, at 2.9 and 4.5 MHz, indicating that the second resonance corresponds to Na in a considerably more distorted coordination polyhedron

than the first. From the values of C_Q, it is possible to assign the resonances as shown in Table 3. The quadrupolar asymmetry parameter (η_Q) of both resonances is 0.0, indicating axial symmetry.

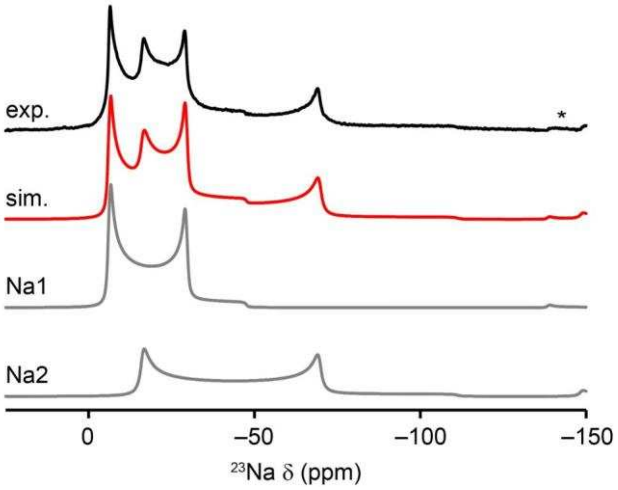

Figure 3: ^{23}Na{^{1}H} (9.4 T 14 kHz MAS) NMR spectrum of BaNaRh(OH)$_6$. The red line indicates the spectrum simulated with the parameters given in Table 3 and the grey lines show the individual contributions to the spectrum. The asterisk denotes a spinning sideband.

Table 3: ^{23}Na NMR parameters for BaNaRh(OH)$_6$

Site	δ_{iso} (ppm)	C_Q / MHz	η_Q
Na1	0.7(1)	2.9(1)	0.0(1)
Na2	–0.2(1)	4.5(1)	0.0(1)

The thermal behaviour of the three hydroxides was investigated using thermodiffraction, Figure 4. This reveals that each hydroxide collapses on heating above 300 °C. Complementary TGA performed on heating in flowing air (Supporting Information) shows that this temperature corresponds to an abrupt mass loss for each material, which most likely corresponds to dehydroxylation.

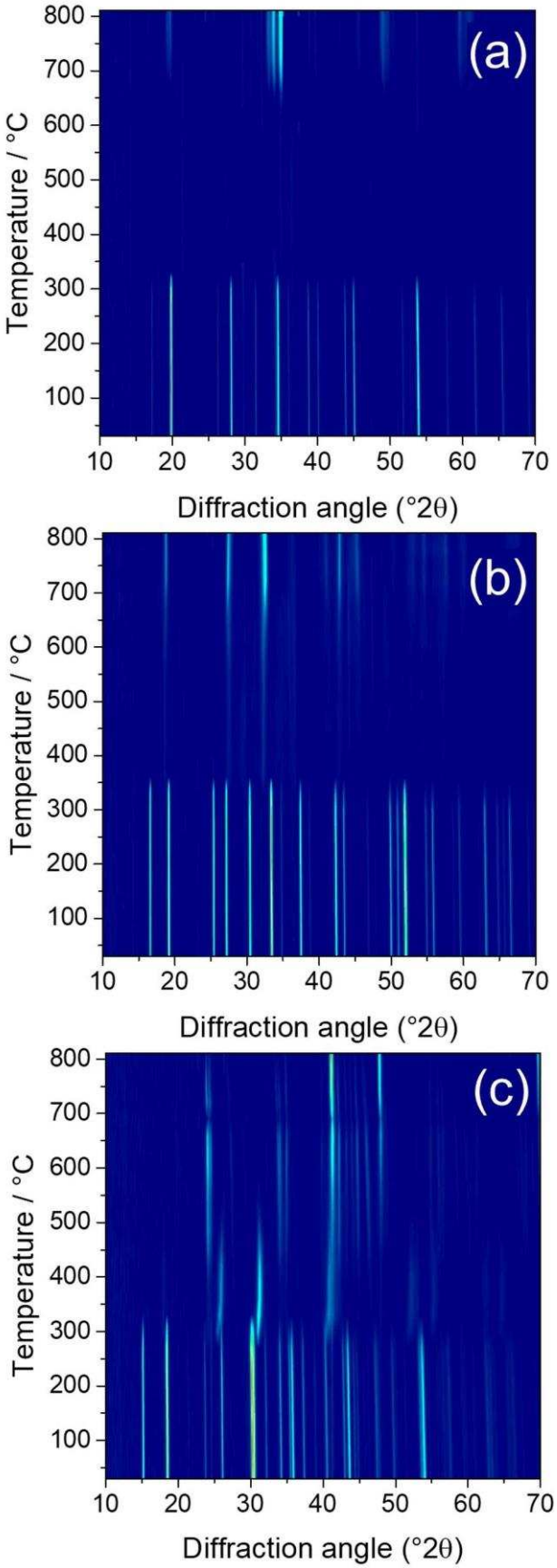

Figure 4: Thermodiffraction data (Cu K_α) for (a) $Ca_3Rh_2(OH)_{12}$, (b) $Sr_3Rh_2(OH)_{12}$ and (c) $BaNaRh(OH)_6$ on heating in flowing air.

In the case of $Ca_3Rh_2(OH)_{12}$, the material produced after continued heating to 800 °C contains the ternary oxide $CaRh_2O_4$ along with CaO (Supporting Information), but after washing with 2 M nitric acid CaO is removed to produce a phase-pure sample of $CaRh_2O_4$, as proven by Rietveld analysis of powder XRD data, Figure 5c and Table 4. The lattice parameters obtained from the refinement are similar to those obtained from a previous single-crystal XRD structure refinement, which was also carried out at room temperature: a = 9.0354(3) Å, b = 3.0340(1) Å, c = 10.7062(3) Å.[26] The material $CaRh_2O_4$ contains both edge- and corner-shared Rh-O octahedra, each of which edge share with 8-coordinate Ca, and is isostructural with $CaFe_2O_4$. Previous reports of the synthesis of $CaRh_2O_4$ used a high-pressure solid-state synthesis from powders of binary oxides at 6 GPa and temperature of 1000 °C for polycrystalline products and 1500 °C for single crystals,[26] or heating of component oxides at 1400 K for 6 days in dry oxygen.[27] Our synthetic route is therefore a much more convenient method and, furthermore, produces a fine-grained powder of crystallites with submicron dimensions, Figures 5a and 5b.

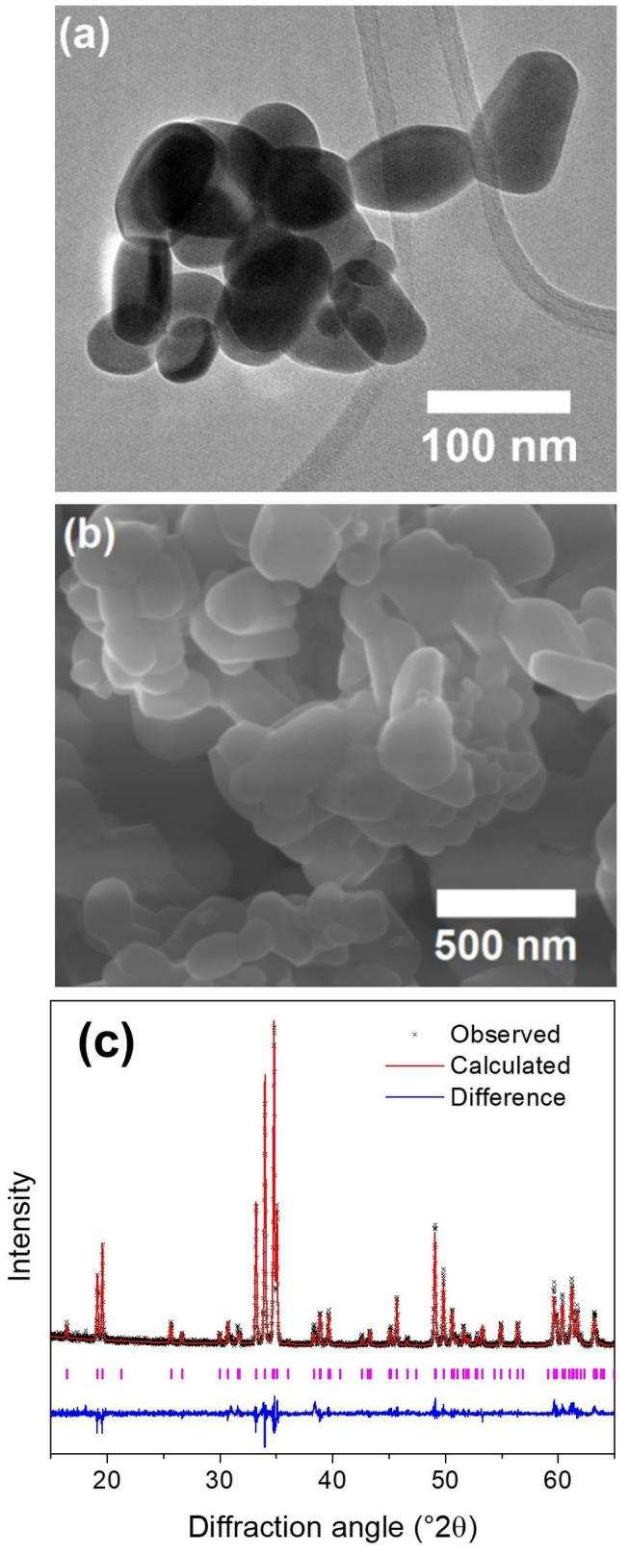

Figure 5: Characterisation of $CaRh_2O_4$ prepared by thermal decomposition of $Ca_3Rh_2(OH)_{12}$. (a) Transmission electron micrograph, (b) Scanning electron micrograph and (c) Rietveld fit to powder XRD pattern (λ = 1.5406 Å).

Table 4: Refined crystal parameters for $CaRh_2O_4$ from powder XRD. Space group *Pnma*, a = 9.0603(2) Å, b = 3.09854(7) Å, c = 10.7809(3) Å. Rp = 14.7%, wRp = 20.5%

Wyckoff Site	Atom	x	y	z	Occupancy	B_{eq} / Å^2
4c	Ca	0.2405(8)	0.25	0.3375(7)	1.0	0.3
4c	Rh	0.0894(3)	0.25	0.5992(3)	1.0	0.3
4c	Rh	0.0558(3)	0.25	0.1151(3)	1.0	0.3
4c	O	0.300(2)	0.25	0.6737(16)	1.0	0.3
4c	O	0.363(2)	0.25	–0.0430(16)	1.0	0.3
4c	O	0.463(2)	0.25	0.2193(17)	1.0	0.3
4c	O	0.110(2)	0.25	–0.0795(15)	1.0	0.3

Thermal decomposition of $Sr_3Rh_2(OH)_{12}$ was described by Ivanov-Emin et al. who reported thermogravimetric analysis.[35] This led the authors to conclude the decomposition product was $SrRh_2O_4$, supported by a similarity of the powder XRD pattern to orthorhombic $SrSc_2O_4$. However, we find for $Sr_3Rh_2(OH)_{12}$ the ultimate product on heating to 800 °C is rather different. Comparing the observed data of the strontium rhodium hydrogarnet decomposition product against strontium rhodates reported in the literature shows that the decomposition product most closely resembles $Sr_6Rh_5O_{15}$, Figure 6. There are other possible candidates for the decomposition product that all have related 2H-perovskite structures and contain mixed-valent $Rh^{3+/4+}$ (Supporting Information). We note that the Sr:Rh ratio in $Sr_6Rh_5O_{15}$ is slightly different to the hydrogarnet and would imply loss of a small amount of Sr in a byproduct. Although the sample formed by thermal decomposition never gave a diffraction pattern of sufficient quality to allow a full structure refinement, evidence for the higher oxidation state of Rh is provided by Rh K-edge XANES spectroscopy, Figure 7. This shows a distinctive shift in edge position to higher energy from that of materials that contain octahedral Rh^{3+}. Attempts improve the crystallinity and resolve the peaks to confirm the phase identification of the product, by heating at above 900 °C in air, resulted in further oxidation to give some Sr_2RhO_4 (Supporting Information), while heating under N_2 resulted in decomposition into rhodium metal. $Sr_6Rh_5O_{15}$ was previously reported to be synthesised as a polycrystalline powder by a solid-state

reaction at 1150 °C for 9 days[13] and as single crystals in a molten potassium carbonate flux at 1050 °C.[43] The different behaviour of the calcium and strontium rhodium hydrogarnets on thermal decomposition is noteworthy, and despite the fact that $SrRh_2O_4$ is known in two polymorphs, with the β-$SrRh_2O_4$ formed on heating $SrCO_3$ and Rh metal in air,[44] instead a mixed-valent Rh^{3+}/Rh^{4+} strontium oxide is formed. The great covalency of strontium compared to calcium may be the origin of the stabilisation of the higher rhodium oxidation state.

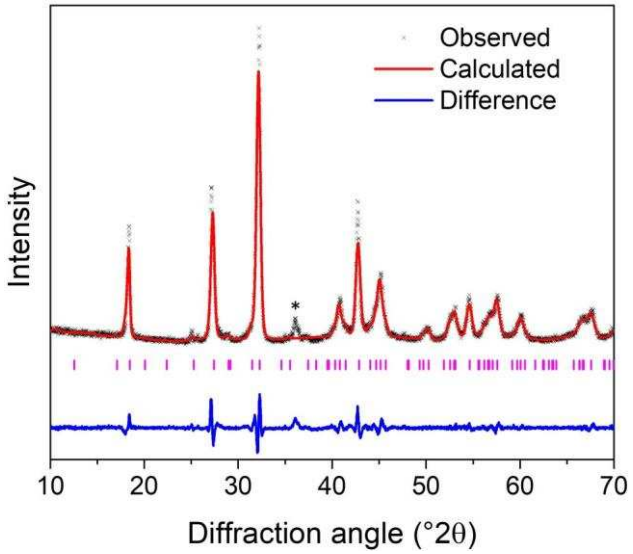

Figure 6: Pawley fit to the powder XRD pattern (Cu K_α) of the Sr-Rh oxide produced by decomposition of $Sr_3Rh_2(OH)_{12}$ using the published single crystal structure model[43] of $Sr_6Rh_5O_{15}$. a = 9.5989(14) Å, c = 13.255(3) Å, R32. Rwp = 14.7%; Rp = 11.4%. An unindexed impurity peak is indicated by the asterisk.

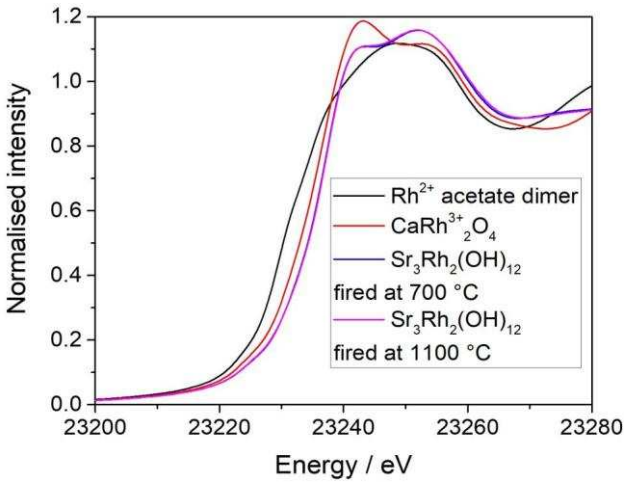

Figure 7: Rh K-edge XANES spectroscopy of the Sr-Rh oxide produced by decomposition of $Sr_3Rh_2(OH)_{12}$, along with Rh^{3+} reference materials and Rh^{2+} acetate dimer.

The thermal decomposition of $BaNaRh(OH)_6$ is more complex than for the hydrogarnets. The thermodiffraction data show the emergence of a transient phase between 325 °C and 500 °C (Figure 4a). A third phase can be seen to form at around 400 °C and remains the only stable phase after heating to 810 °C. As yet, no candidate structure for this last material has been identified, though the observed reflections are similar in position and intensity to $Sr_6Rh_5O_{15}$, but shifted to lower angle consistent with the presence of the larger Ba^{2+} cation in a similar hexagonal perovskite structure.

Conclusions

Investigtaion of the hydrothermal chemistry of Rh^{3+} in alkali solutions allows the crystallisation of mixed-metal hydroxide materials, including some hydrogarnets and a new barium-sodium-rhodium hydroxide. The same phases are formed even if peroxides are used as the reagents, which contrasts with the chemistry of other platinum-group materials, such as Ru or Ir, where higher oxidation states are stabilised in oxide products under similar conditions. The complex rhodium hydroxides can, however, be decomposed under moderate temperatures to yield oxide phases that have only previously been reported to form under extreme conditions of high pressure and/or temperature in oxygen atmosphere (in the case of $CaRh_2O_4$) and molten fluxes (in the case of hexagonal strontium rhodate perovskites). As well as a potential route to materials with interesting

properties, this widens the possibility of using the formation of metastable mixed-metal hydroxides to isolate difficult-to-prepare, or new, oxide materials under moderate reaction conditions and in future work extending these ideas to more chemically diverse systems, such as mixed 3d-4d oxides, could be fruitful.

Supporting Information Available: further powder diffraction data and thermogravimetric analysis.

CCDC 1852391 contains the supplementary single-crystal crystallographic data for this paper. These data can be obtained free of charge via www.ccdc.cam.ac.uk/data_request/cif, or by emailing data_request@ccdc.cam.ac.uk, or contacting The Cambridge Crystallographic Data Centre, 12 Union Road, Cambridge CB2 1EZ, UK; fax: +44 1223 336033.

Acknowledgements

DSC thanks Johnson Matthey for the award of a CASE studentship. We thank Diamond Light Source for provision of beamtime for XANES as part of the Energy Materials Block Allocation Group SP14239. The I11 beamtime was obtained through the Diamond Light Source Block Allocation Group award "Oxford Solid State Chemistry BAG to probe composition-structure-property relationships in solids" (EE13284) and we thank Dr Mark Senn and Mr Gabriel Clarke for their assistance with measuring the data. We are grateful to Mr James Crosland for the TGA analysis.

References

1. Biesterbos, J. W.; Hornstra, J., Crystal-Structure of High-Temperature, Low-Pressure Form of Rh_2O_3. J. Less-Common Met. **1973,** 30, 121-125.
2. Bayer, G.; Wiedemann, H. G., Formation and Thermal-Stability of Rhodium Oxides. Thermochim. Acta **1976,** 15, 213-226.
3. Poeppelmeier, K. R.; Ansell, G. B., Growth of the High-Temperature, High-Pressure Polymorph of Rh_2O_3 by Chemical-Transport with HCl. J. Cryst. Growth **1981,** 51, 587-588.
4. Muller, O.; Roy, R., Formation and Stability of the Platinum and Rhodium Oxides at High Oxygen Pressures and the Structures of Pt_3O_4, β–PtO_2 And RhO_2. J. Less-Common Met. **1968,** 16, 129–146.
5. Shannon, R. D., Synthesis and Properties of Two New Members of the Rutile Family RhO_2 and PtO_2. Solid State Commun. **1968,** 6, 139–143.
6. Müller-Buschbaum, H., On the Crystal Chemistry of Oxorhodates. Z. Anorg. Allg. Chem. **2007,** 633, 1289-1306.
7. Chamberland, B. L.; Anderson, J. B., The Preparation and Crystal-Structure of a $BaRhO_3$ Polytype. J. Solid State Chem. **1981,** 39, 114-119.
8. Stitzer, K. E.; Smith, M. D.; Darriet, J.; zur Loye, H. C., Crystal Growth, Structure Determination and Magnetism of a New Hexagonal Rhodate: $Ba_9Rh_8O_{24}$. Chem. Commun. **2001**, 1680-1681.
9. Shimura, T.; Itoh, M.; Nakamura, T., Novel 2-Dimensional Conductor Sr_2RhO_4. J. Solid State Chem. **1992,** 98, 198-200.
10. Yamaura, K.; Huang, Q.; Young, D. P.; Noguchi, Y.; Takayama-Muromachi, E., Crystal Structure and Electronic and Magnetic Properties of the Bilayered Rhodium Oxide $Sr_3Rh_2O_7$. Phys. Rev. B **2002,** 66.
11. Reisner, B. A.; Stacy, A. M., Sr_3ARhO_6 (A = Li, Na): Crystallization of a Rhodium(V) Oxide from Molten Hydroxide. J. Am. Chem. Soc. **1998,** 120, 9682-9683.
12. Mugavero, S. J.; Gemmill, W. R.; Roof, I. P.; zur Loye, H. C., Materials Discovery by Crystal Growth: Lanthanide Metal Containing Oxides of the Platinum Group Metals (Ru, Os, Ir, Rh, Pd, Pt) from Molten Alkali Metal Hydroxides. J. Solid State Chem. **2009,** 182, 1950-1963.
13. Claridge, J. B.; zur Loye, H. C., Synthesis, Structure, and Magnetic Properties of a Novel Mixed-Valent Strontium Rhodium Oxide. Chem. Mater. **1998,** 10, 2320-2322.
14. Saeed, Y.; Singh, N.; Schwingenschlogl, U., Superior Thermoelectric Response in the 3R Phases of Hydrated Na_xRhO_2. Sci. Rep. **2014,** 4, 4390.
15. Park, J. E.; Hu, Y.; Krizan, J. W.; Gibson, Q. D.; Tayvah, U. T.; Selloni, A.; Cava, R. J.; Bocarsly, A. B., Stable Hydrogen Evolution from an $AgRhO_2$ Photocathode under Visible Light. Chem. Mater. **2018,** 30, 2574–2582.
16. Sardar, K.; Fisher, J.; Thompsett, D.; Lees, M. R.; Clarkson, G. J.; Sloan, J.; Kashtiban, R. J.; Walton, R. I., Structural Variety in Iridate Oxides and Hydroxides from Hydrothermal Synthesis. Chem. Sci. **2011,** 2, 1573-1578.
17. Hiley, C. I.; Lees, M. R.; Fisher, J. M.; Thompsett, D.; Agrestini, S.; Smith, R. I.; Walton, R. I., Ruthenium(V) Oxides from Low-Temperature Hydrothermal Synthesis. Angew. Chem.- Int. Ed. **2014,** 53, 4423-4427.
18. Hiley, C. I.; Walton, R. I., Controlling the Crystallisation of Oxide Materials by Solvothermal Chemistry: Tuning Composition, Substitution and Morphology of Functional Solids. CrystEngCommun **2016,** 18, 7656-7670.
19. Hiley, C. I.; Scanlon, D. O.; Sokol, A. A.; Woodley, S. M.; Ganose, A. M.; Sangiao, S.; De Teresa, J. M.; Manuel, P.; Khalyavin, D. D.; Walker, M.; Lees, M. R.; Walton, R. I., Antiferromagnetism at T > 500 K in the Layered Hexagonal Ruthenate $SrRu_2O_6$. Phys. Rev. B **2015,** 92, 104413

20. Hiley, C. I.; Lees, M. R.; Hammond, D. L.; Kashtiban, R. J.; Sloan, J.; Smith, R. I.; Walton, R. I., $Ba_4Ru_3O_{10.2}(OH)_{1.8}$: A New Member of the Layered Hexagonal Perovskite Family Crystallised from Water. Chem. Commun. **2016,** 52, 6375-6378.
21. Sardar, K.; Petrucco, E.; Hiley, C. I.; Sharman, J. D. B.; Wells, P. P.; Russell, A. E.; Kashtiban, R. J.; Sloan, J.; Walton, R. I., Water-Splitting Electrocatalysis in Acid Conditions Using Ruthenate-Iridate Pyrochlores. Angew. Chem.- Int. Ed. **2014,** 53, 10960-10964.
22. Prasad, B. E.; Kazin, P.; Komarek, A. C.; Felser, C.; Jansen, M., β-Ag_3RuO_4, a Ruthenate(V) Featuring Spin Tetramers on a Two-Dimensional Trigonal Lattice. Angew. Chem.- Int. Ed. **2016,** 55, 4467-4471.
23. Prasad, B. E.; Kanungo, S.; Jansen, M.; Komarek, A. C.; Yan, B. H.; Manuel, P.; Felser, C., $AgRuO_3$, a Strongly Exchange-Coupled Honeycomb Compound Lacking Long-Range Magnetic Order. Chem. Eur. J. **2017,** 23, 4680-4686.
24. Kurzman, J. A.; Misch, L. M.; Seshadri, R., Chemistry of Precious Metal Oxides Relevant to Heterogeneous Catalysis. Dalton Trans. **2013,** 42, 14653-14667.
25. Witczak-Krempa, W.; Chen, G.; Kim, Y. B.; L. Balents, Correlated Quantum Phenomena in the Strong Spin-orbit Regime. Annu. Rev. Condens. Matter Phys. **2014,** 5, 57–82.
26. Yamaura, K.; Huang, Q.; Moldovan, M.; Young, D. P.; Sato, A.; Baba, Y.; Nagai, T.; Matsui, Y.; Takayama-Muromachi, E., High-pressure Synthesis, Crystal Structure Determination, and a Ca Substitution Study of the Metallic Rhodium Oxide $NaRh_2O_4$. Chem. Mater. **2005,** 17, 359-365.
27. Jacob, K. T.; Waseda, Y., Solid state cells with buffer electrodes for measurement of chemical potentials and Gibbs energies of formation: System Ca-Rh-O. J. Solid State Chem. **2000,** 150, 213-220.
28. Moran-Miguelez, E.; Alario-Franco, M. A., Hydrothermal Synthesis and Reactivity of Rhodium Dioxide and Oxyhydroxide. Thermochim. Acta **1983,** 60, 181-186.
29. Thompson, S. P.; Parker, J. E.; Potter, J.; Hill, T. P.; Birt, A.; Cobb, T. M.; Yuan, F.; Tang, C. C., Beamline I11 at Diamond: A New Instrument for High Resolution Powder Diffraction. Rev. Sci. Instrum. **2009,** 80.
30. Coelho, A. A., TOPAS And TOPAS-Academic: An Optimization Program Integrating Computer Algebra and Crystallographic Objects Written in C Plus. J. Appl. Cryst. **2018,** 51, 210-218.
31. Sheldrick, G. M., SHELXT - Integrated Space-group and Crystal-structure Determination. Acta Crystallogr. Sect. A **2015,** 71, 3-8.
32. Sheldrick, G. M., Crystal structure refinement with SHELXL. Acta Crystallogr. Sect. C **2015,** 71, 3-8.
33. Dent, A. J.; Cibin, G.; Ramos, S.; Smith, A. D.; Scott, S. M.; Varandas, L.; Pearson, M. R.; Krumpa, N. A.; Jones, C. P.; Robbins, P. E., B18: A Core XAS Spectroscopy Beamline for Diamond. Phys. Conf. Ser. **2009,** 190, 012039
34. Ravel, B.; Newville, M., ATHENA, ARTEMIS, HEPHAESTUS: Data Analysis for X-ray Absorption Spectroscopy Using IFEFFIT. J Synchrotron Radiat. **2005,** 12, 537-541.
35. Ivanov-Emin, B. N.; Nevskaya, N. A.; Zaitsev, B. E.; Tsirel'nikov, V. I., The Synthesis and Study of Strontium Hexahydroxorhodate. Russ. J. Inorg. Chem, **1983,** 28, 557.
36. Morán-Miguélez, E.; Alario-Franco, M. A.; Joubert, J. C., Hydrothermal Synthesis and Field of Existence of Silicon-Free Hydrogarnets. Mater. Res. Bull. **1986,** 21, 107-113.
37. Nevskii, N. N.; Ivanovemin, B. N.; Nevskaia, N. A.; Kaziev, G. Z.; Belov, N. V., Crystal-Structure of Strontium Hydrogarnets. Dokl. Akad. Nauk SSSR **1982,** 264, 857-858.
38. Shannon, R. D., Revised Effective Ionic Radii and Systematic Studies of Interatomic Distances in Halides and Chalcogenides. Acta Crystallogr. **1976,** A32, 751-767.
39. Brown, I. D.; Altermatt, D., Bond-Valence Parameters Obtained from a Systematic Analysis of the Inorganic Crystal-Structure Database. Acta Crystallogr. Sect. B **1985,** 41, 244-247.
40. Kwestroo, W.; van Gerven, H. C. A.; van Hal, H. A. M., Hydrogarnets $Ba_3In_2(OH)_{12}$ and $Ba_3Sc_2(OH)_{12}$. Mater. Res. Bull. **1977,** 12, 161-164.
41. Chance, W. M.; Bugaris, D. E.; Sefat, A. S.; zur Loye, H. C., Crystal Growth of New Hexahydroxometallates Using a Hydroflux. Inorg. Chem. **2013,** 52, 11723-11733.

42. Mizoguchi, H.; Bhuvanesh, N. S. P.; Kim, Y. I.; Ohara, S.; Woodward, P. M., Hydrothermal Crystal Growth and Structure Determination of Double Hydroxides $LiSb(OH)_6$, $BaSn(OH)_6$, and $SrSn(OH)_6$. Inorg. Chem. **2014,** 53, 10570-10577.
43. Stitzer, K. E.; El Abed, A.; Darriet, J.; zur Loye, H. C., Growth of $Sr_6Rh_5O_{15}$ Single Crystals from High-Temperature Solutions: Structure Determination using the Traditional 3-D and the 4-D Superspace Group Methods and Magnetic Measurements on Oriented Single Crystals. J. Am. Chem. Soc. **2001,** 123, 8790-8796.
44. Hector, A. L.; Levason, W.; Weller, M. T., Structure of β-$SrRh_2O_4$ from X-ray and neutron powder diffraction Eur. J. Solid State Inorg. Chem. **1998,** 35, 679-687.

For Table of Contents Only

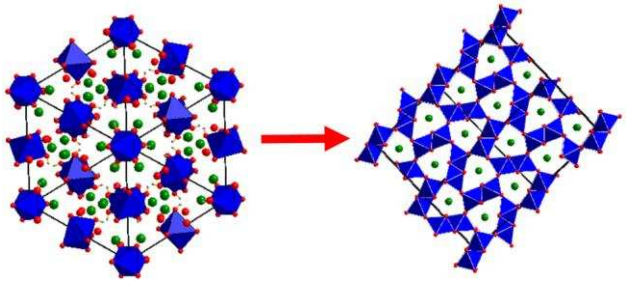

Subcritical hydrothermal reactions of Rh^{3+} in alkali-earth hydroxides yields various mixed-metal rhodium hydroxides whose structures have been determined: subsequent thermal decomposition at moderate temperatures forms ternary rhodium oxides that usually require extreme temperatures or oxygen atmospheres by conventional solid-state synthesis.